Article

Journal of the Brazilian Chemical Society

https://dx.doi.org/10.21577/0103-5053.20240002

J. Braz. Chem. Soc. **2024**, *35*, 6, e-20240002, 1-11

Magnetic Crosslinked Porcine Pancreatic Lipase Aggregates for Transesterification Process

Caroline O. da Rocha,[a] Rodolfo D. Piazza,[a] Caio C. dos Santos,[a] Guilherme N. Lucena,[a] Bruno E. Amantea,[a] Miguel Jafelicci Jr.,[a] Ariela V. de Paula,[b,c] Anselmo F. Ruiz Rodriguez,[d] Marco Antonio Morales[e] and Rodrigo Fernando C. Marques[*,a,c,f]

[a]*Laboratório de Materiais Magnéticos e Coloides, Departamento de Química Analítica, Físico Química e Química Inorgânica, Instituto de Química, Universidade Estadual Paulista (UNESP), 14800-060 Araraquara-SP, Brazil*

[b]*Faculdade de Ciências Farmaceuticas, Universidade Estadual Paulista (UNESP), 14800-903 Araraquara-SP, Brazil*

[c]*Instituto de Pesquisa em Bioenergia (IPBEN), Instituto de Química, Universidade Estadual Paulista (UNESP), 14800-060 Araraquara-SP, Brazil*

[d]*Laboratório de Nanobiotecnologia, Universidade Federeal do Acre, 69920-900 Rio Branco-AC, Brazil*

[e]*Departamento de Física Teorica e Experimental, Universidade Federal do Rio Grande do Norte, 59078-970 Natal-RN, Brazil*

[f]*Centro de Monitoramento e Pesquisa da Qualidade de Combustíveis, Petróleo e Derivados (CEMPEQC), Instituto de Química, Universidade Estadual Paulista (UNESP), 14800-060 Araraquara-SP, Brazil*

Lipases have been used in industrial processes as biocatalysts for transesterification reactions. The synergism between enzymes and magnetic properties may be reached by using magnetic nanoparticles (MNPs) as support to immobilize them in aggregate structures, denominated by magnetic crosslinked enzyme aggregates (MCLEA). One of the advantages of such supports is the possibility of using magnetic separation for enzyme recovery, reducing costs and allowing reuse in continuous systems. Here, porcine pancreatic lipase (PPL) was immobilized onto functionalized magnetite support (Fe_3O_4-APTS) with a protein binding efficiency of 78.84%. Physical and chemical properties of the nanoparticles and immobilized lipase were characterized by X-ray diffraction (XDR), transmission electron microscopy (TEM), infrared spectroscopy (FTIR), dynamic light scattering (DLS), zeta potential, vibrating sample magnetometer measurements (VSM), and ^{57}Fe Mössbauer spectroscopy. The immobilized lipase additionally exhibited improved stability across wide pH and temperature ranges compared with free lipase. The immobilized derivate also attained good reusability, maintaining 61.37% of its initial activity after 6 reaction cycles. Through magnetic behavior and also because of its surface modification to crosslinking the enzyme, the MCLEA produced in this work has enhanced the biocatalytic activities of PPL.

Keywords: immobilization, porcine pancreatic lipase, magnetic nanoparticles, hydrolytic activity, MCLEA

Introduction

Enzymes are applied efficiently in different sectors such as the food and pharmaceutical industries.[1] Currently, there is great interest in the use of enzymes in the production of biofuels as many chemical reactions can render them economically competitive.[2-6] According to the support and production method selected, the activity and reusability of the enzyme are strongly influenced,[7,8] conferring greater stability and resistance across different pH and temperature ranges, in addition to preserving enzyme activity over several catalytic cycles.[9]

For the biocatalysts to succeed, the support must be inert and compatible with the enzyme and must not interfere with its native protein structure or compromise its biological

*e-mail: costa.marques@unesp.br
Editor handled this article: Izaura C. N. Diógenes (Associate)

activity.[10] The best support options are solid carriers that interact with the enzyme by adsorption, covalent bonding, encapsulating, confinement, or crosslinking.[11,12] Previous studies[13] have indicated that carbon nanotubes, silica mesopores, nanofibers, nanocomposites, nanorods, and magnetic nanoparticles (MNPs) are all feasible nanomaterials for support.

Among the different supports, magnetite nanoparticles (Fe_3O_4) emerge as a promising material that plays an essential role in enzyme immobilization. Fe_3O_4 is colloidally stable, exhibits good liquid dispersion, and may be easily applied on an industrial scale.[14-16] However, Fe_3O_4 nanoparticles are prone to oxidation in the environment necessary for reactions, so a protective shell of silica or other inert material is required to achieve chemical stability.[17,18] Furthermore, Fe_3O_4 can be functionalized with a wide range of functional groups capable of immobilizing enzymes on its surface, without losing the magnetic properties that allow easy separation from the reaction medium through an external magnetic field.[19]

Lipases have been the most used biocatalysts in industrial processes. They can be applied in several types of industries, being one of the most historically important groups of biocatalysts for biotechnological applications.[20,21] They found applications in synthesizing fine chemicals, such as agrochemicals, therapeutics, cosmetics, and flavors; new biopolymeric materials, and biodiesel production.[19]

Lipases (E.C.3.1.1.3) are classified as hydrolases, mainly hydrolyzing triglycerides (TAGs) to glycerol and fatty acids.[22] These enzymes are classified based on their origin: plant, animal, and microbial lipases. Animal lipase is low-cost and obtained from the pancreas of cattle, sheep, or swine.[23] Lipases operate at the interface between lipids and water and therefore possess an α-helical amphipathic 'cap' region of the protein that covers the catalytic residues of the active site.[23] A closed cap protects the active site from the environment and makes interaction with the substrate impossible; an open cap allows the protein to perform its catalytic activity.[24]

Crosslinked enzyme aggregates (CLEAs) are an excellent technology for the immobilization of enzymes that, when used in conjunction with surface-functionalized magnetic nanoparticles, can form magnetic crosslinked enzyme aggregates (MCLEAs).[25] In addition to the biocatalytic properties of CLEAs, such as increasing enzyme thermostability compared to free enzymes,[26] MCLEAs add the magnetic properties of Fe_3O_4 nanoparticles, becoming advantageous during magnetic separation. Other advantages of using MCLEAs include a higher proportion of enzyme-substrate, improved reusability, reduced chance of contamination, improvements in activity, process control, catalytic process, functional effectiveness, product stability, and level of continuous operation.[27]

Some scientific literature has already described the immobilization of porcine pancreatic lipase (PPL) with a magnetic carrier and characterized hydrolytic activity in olive oil,[28,29] however, the use of MNPs to immobilize a PPL enzyme was not discussed based on its magnetic properties. This work aimed to evaluate the immobilization of PPL onto MNPs and its application in biocatalysts reactions. The hydrolytic activity was evaluated for free and immobilized PPL to determine the catalytic viability of immobilized PPL in the transesterification of olive oils to produce biodiesel. The enzyme aggregates obtained in this work have demonstrated that the concept test of these magnetic supports and their crosslinking with the enzyme lead to cutting-edge materials that will certainly improve biodiesel synthesis.

Experimental

Chemicals

Iron(II) chloride tetrahydrate ($FeCl_2.4H_2O$), iron(III) chloride hexahydrate ($FeCl_3.6H_2O$), diethanolamine (DEA), diethylene glycol (DEG), glutaraldehyde (25%), phosphate buffer (pH 7.4), porcine pancreatic lipase (PPL), polyethyleneglycol (1×10^6 g mol^{-1}), 3-aminopropyltriethoxysilane (APTS) and gum arabic powder were purchased from Sigma-Aldrich Co. (Burlington, USA). Sodium hydroxide (NaOH) and commercial ethanol were purchased from Synth (São Paulo, Brazil). Sodium chloride was purchased from J. T. Baker, S.A. (Phillipsburg, USA).

Synthesis of MNPs functionalized with amine group

The Fe_3O_4 MNPs were obtained by the precipitation in alkali media. Briefly, 2 mmol of $FeCl_2.4H_2O$ and 4 mmol of $FeCl_3.6H_2O$ were dissolved in 80 mL of DEG/DEA (1:1, v/v) and, separately, 16 mmol of NaOH was dissolved in 80 mL of DEG/DEA (1:1, v/v). The solutions were magnetically stirred in a round flask, under an argon atmosphere. The reaction took place at 200 °C for 8 h. After cooling to ambient temperature, the black precipitate was centrifuged and washed with alcohol/water (1:1, v/v) three times. Then, the sample was dried in a dissector and denominated by Fe_3O_4.[30]

For functionalization, 200 µL of APTS were added to 20 mL of Fe_3O_4 suspension. The system was magnetically stirred for 24 h and then centrifuged and washed with alcohol/water (1:1, v/v) three times. The precipitate was denominated by Fe_3O_4-APTS.

MCLEAs obtention

An aliquot of 5 mL of Fe_3O_4-APTS (0.9 g mL^{-1}) was added to a Falcon tube containing 18 mL of phosphate buffer (0.01 mol L^{-1}, pH 7.4). Subsequently, 2 mL glutaraldehyde (25%) were added and the solution was vortexed for 1 h, at room temperature, to obtain the aggregate structures. The system was centrifuged and the precipitate was washed with alcohol, water, and phosphate buffer solution (1:1:1) to remove any excess glutaraldehyde, at least 10 times until the supernatant turns colorless. Then, the magnetic aggregate was suspended in 20 mL of phosphate buffer, followed by the addition of 50 mg of PPL and 0.01 g of polyethylene glycol (1000 kDa). Vortexing was performed for 5 min before the solution was maintained for 16 h at 6 °C. The suspension was centrifuged and the precipitate was washed with phosphate buffer (pH 8.0, 1 mol L^{-1}) to remove any free PPL. The sample was denominated by Fe_3O_4-PPL.

Enzymatic immobilization yield

The immobilization yield was evaluated through protein dosage carried out by Bradford assay, according to a previous work.[31] Equation 1 was employed for immobilization yield determination:

$$\text{Immobilization yield}(\%) = \left(1 - \frac{P_f}{P_i}\right) \times 100 \quad (1)$$

where P_f corresponds to the protein concentration of free PPL and P_i is the protein concentration of the immobilized Fe_3O_4-PPL sample.

Hydrolytic activity of lipase immobilized with MNPs

The hydrolytic activity was determined by the olive oil emulsion method proposed by Bassan *et al.*[30] 2.5 mL of olive oil and water emulsion (1:1 v/v) and 2 mL of phosphate buffer (0.1 mol L^{-1}, pH 8.0) were mixed. The reaction media was kept under stirring at 150 rpm in a thermostatic bath. 2 mL of the immobilized enzyme solution (1 mg mL^{-1}) were added, keeping the system under stirring at 37 °C for 5 min. After the incubation period, 10 mL of a mixture of ethanol and acetone (1:1) and 10 mL of a previously standardized KOH solution (0.05 mol L^{-1}) were added. Excess KOH was titrated with HCl (0.05 mol L^{-1}). The enzymatic activity was calculated according to equation 2:

$$A = \frac{(V_b - V_a) \times M \times 10^{-6}}{t \times m} \quad (2)$$

where A is the hydrolytic activity (U g^{-1}), M is the molarity of the HCl solution (mol L^{-1}), t is the incubation time (min), V_b is the blank volume (L), V_a is the sample volume (L) and m is the mass of the biocatalyst (g).

Determination of the optimum pH and temperature

To study the influence of pH on free and immobilized lipase, the analyses were carried out at a constant 37 °C, varying the buffer's pH from 3 to 10. After establishing the optimum pH value of the enzyme, the pH was kept constant and the temperatures were evaluated between 30 and 60 °C to determine the optimum temperature for biocatalyst activity.[30] Na_2HPO_4 (0.1 M) and citric acid (0.1 M) were employed to prepare a buffered solution comprising between pH 3.0 to 8.0. Buffers made from Na_2CO_3 (0.1 M) and Na_2HPO_4 (0.1 M) were used for pH range of 9 and 10.

Thermal stability

To compare thermal stability, free and immobilized enzymes were incubated in 1 mL of phosphate buffer (0.1 mol L^{-1}) at pH 7.0 and pH 8.0, respectively, at 60 ºC for 4, 8, 12, and 24 h. Storage stability and reaction temperature of free and immobilized preparations were studied during storage at 4 ºC and at reaction time by evaluating their activity for 4, 8, 12, and 24 h.[25] The reusability of the enzyme was evaluated in the transesterification reaction of olive oil. After reaction at 60 ºC, the immobilized derivative was separated by a magnet and washed three times with *n*-hexane and then three times with water. After this treatment, the immobilized enzyme was resuspended in a new aliquot of substrates for the next catalytic cycle.

Instrumentation

The Fourier transform infrared (FTIR) spectra were recorded by a PerkinElmer Frontier model spectrometer (Waltham, USA), equipped with attenuance total reflectance (zinc selenide crystal) apparatus. Spectra were recorded by 128 scans, with 4 cm^{-1} resolution. Transmission electron microscopy (TEM) analysis was carried out with a Philips CM120 microscope (Amsterdam, Netherlands). The software ImageJ (version 1.45s)[32] was used for image treatment. The X-ray diffraction (XRD) patterns of samples were obtained in a Siemens D5005 diffractometer (Berlin, Germany) using Kα radiation, with a wavelength (λ) of 0.15418 nm. Measurements were recorded at the 2θ scan interval from 10 to 80°, with a scan speed of 0.02° *per* second. The thermogravimetric

analysis (TG) of the samples was performed on Netzsch STA 409/CD equipment (Ulm, Germany) under dry airflow of 100 mL min^{-1}. Zeta potential was determined by the Zetasizer Nano ZS, Malvern (Malvern, UK). The samples were dispersed in an aqueous solution of 0.001 mol L^{-1} NaCl and titrated in the pH range of 3 to 10. The hydrodynamic diameter was determined by the Zetasizer Nano ZS, Malvern (Malvern, UK), by dynamic light scattering (DLS) technique, which samples were dispersed in deionized water (free PPL sample was previously filtered before measurement). The magnetization measurements were performed in a vibrating sample magnetometer (VSM) from LakeShore, model 7400 (Westerville, USA), at 300 K. The Mössbauer spectra were recorded at 300 K in a spectrometer from SEECo (Westerville, USA) operating in the transmission mode, using a ^{57}Co gamma-ray radiation source with 12 mCi activity. The spectra were fit using Normos90 software;[33] the isomer shifts are reported relative to α-Fe at 300 K.

Results and Discussion

Characterization of lipase immobilization onto magnetic nanoparticle support

The X-ray diffractogram patterns from synthesized (Fe_3O_4), functionalized (Fe_3O_4-APTS), and immobilized (Fe_3O_4-PPL) samples are shown in Figure 1. The X-ray diffraction peaks correspond to the inverse-spinel structure magnetite, consistent with its standard structure (JCPDS card No. 39-1346), and no secondary phase was observed. The estimative of crystallite diameter was calculated from the Scherrer equation, finding 9.75 nm for Fe_3O_4, 9.94 nm for Fe_3O_4-APTS, and 10.17 nm for Fe_3O_4-PPL samples. The samples showed crystallite sizes close to the bare nanoparticles (NPs). It is known that the APTS functionalization molecules are covalently bonded to the surface of the nanoparticles, thus, the chemical modification of the NPs surface may lead to a thin layer of a different iron oxide. According to the X-ray diffractogram patterns, for all samples, and within the XRD sensitivity, we conclude that there are no second phases.

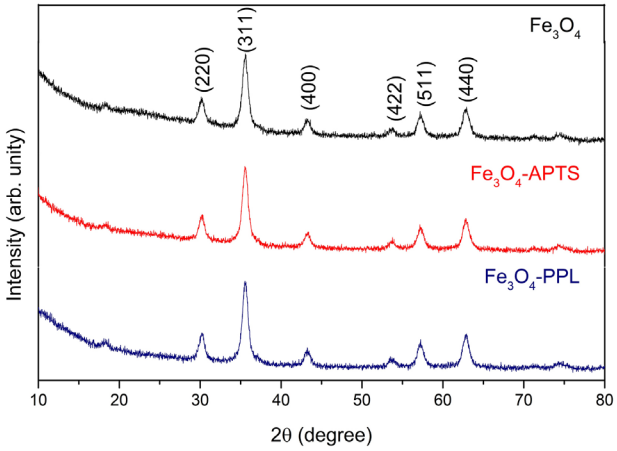

Figure 1. XRD pattern of Fe_3O_4, Fe_3O_4-APTS, and Fe_3O_4-PPL.

The TEM image of Fe_3O_4-APTS particles is shown in Figure 2a. This micrograph displays sphere-like NPs which are homogeneous in shape and size. Figure 2b shows the histogram of nanoparticle sizes. The sizes of 135 NPs were evaluated and the data of frequency *versus* size was fit to a lognormal distribution. The average nanoparticle size was found to be approximately 5.1 nm. The results obtained from XRD and TEM analyses are in accordance with the data reported in the scientific literature.[34,35] Based on the results obtained from XRD regarding the crystallite size, which refers to the average size of individual crystallites in a solid material and are due to pertains to the smallest crystal or polycrystalline solid comprising the crystalline structure, it is observed that this size is slightly larger than

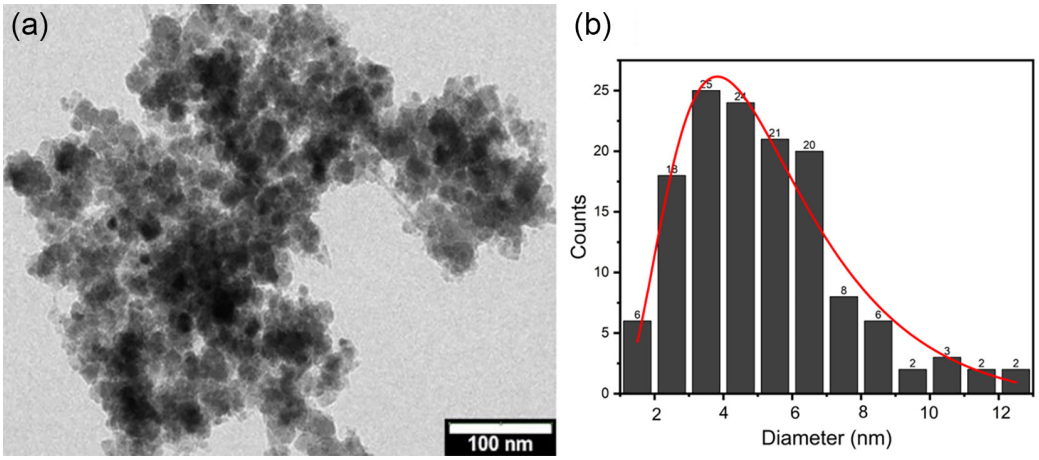

Figure 2. (a) TEM images of Fe_3O_4-APTS sample. (b) Histogram distribution of Fe_3O_4-APTS.

the average particle diameter found in TEM. A particle is composed of aggregated multiple crystals, and when it is small enough, it can refer to a single crystal. Thus, the average particle size is never smaller than the crystallite size. The underestimated average value in TEM is primarily attributed to the limited number of counts and the presence of aggregates, which hinders the accurate determination of the real size of nanoparticles. However, considering the obtained standard deviation, it is evident that the values are convergent.

Since the magnetic core structure was preserved after the functionalization steps, the surface modification was evaluated by FTIR, as shown in Figure 3. For the Fe_3O_4 sample, the bands observed at ca. 3200 and ca. 1600 cm^{-1} were attributed to the presence of water (O–H stretching, H–O–H deformation, respectively). The intense bands observed at 597 and 445 cm^{-1} were attributed to the characteristic Fe–O bond of iron oxide.[36] After APTS functionalization, a significant increase in the intensity of the bands at ca. 3395 and 1625 cm^{-1} was observed and a broadening and displacement can be ascribed to an increase in the contribution of O–H groups derived from silanol and to the N–H folding of primary amines present in the APTS molecule. The bands at 2922 and 2853 cm^{-1} were attributed to symmetric and asymmetric stretching of C–H, as well as the weak bands in the regions 1450 and 1384 cm^{-1} were assigned to C–H folding. A weak and broad band observed in the region 1065 cm^{-1} was attributed to the *ν*Si–O stretching, corroborating the formation of a Si–O coating on the surface of MNPs.[37] After functionalization with the PPL enzyme, a broader and more intense band at ca. 3450 cm^{-1} was observed as a result of the contributions of O–H and N–H bonds caused by the presence of the enzyme, as well as a significant increase in the bands of C–H. In addition, the main bands associated with proteins were observed on free PPL and Fe_3O_4-PPL samples, such as amine I (ca. 1641 cm^{-1}), amide II (ca. 1560 cm^{-1}), and amide III (ca. 1400-1200 cm^{-1}).[38-40] No additional band was observed on the Fe_3O_4-PPL sample, once the crosslinking reaction between aldehyde groups from glutaraldehyde and amine groups from PPL and Fe_3O_4-APTS sample took place on the same absorption region from proteins. However, the primary amine (N–H stretching at 3550 cm^{-1}) is observed only in the free PPL sample. As the primary amine is consumed by the crosslinking step, this band is suppressed and cannot be identified in the Fe_3O_4-PPL sample spectrum.

Zeta potential was also used to assess surface functionalization. Figure 4 depicts the zeta potential of the samples as a function of pH. The isoelectric point (IEP) for the Fe_3O_4 sample is 2.9. Due to surface modification with APTS, the IEP for Fe_3O_4-APTS shifted to 6.4, as

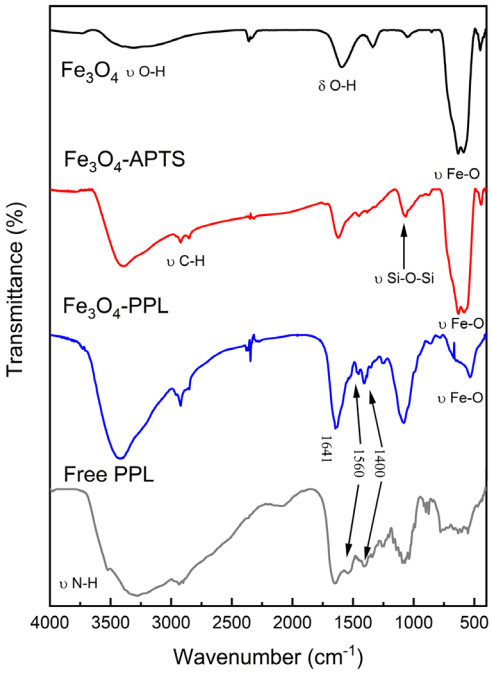

Figure 3. FTIR-ATR spectra of Fe_3O_4, Fe_3O_4-APTS, Fe_3O_4-PPL, and free PPL samples.

expected for the increase in the density of amino groups on the surface of the nanoparticles.[41] Free PPL has an IEP of 5.4, a value close to the immobilized sample (IEP = 5.0). The changes in zeta potential features are caused by the functional groups identified by FTIR measurements for each nanoparticle functionalization step, corroborating both findings.

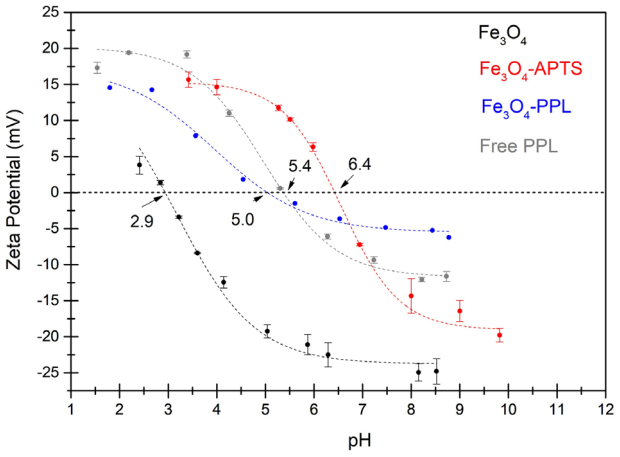

Figure 4. Zeta potential of Fe_3O_4, Fe_3O_4-APTS, Fe_3O_4-PPL, and free PPL.

The average hydrodynamic diameter and polydispersity index (PDI) are summarized in Table 1, meanwhile, Figure 5 shows the distribution profile, which presents a single population for all functionalization steps. The aggregate Fe_3O_4 sample shows an average hydrodynamic diameter of 234.1 nm. The hydrodynamic diameter

increases to 554.1 nm upon functionalization with APTS, due to the growth of silica shell on the nanoparticle surface. Furthermore, the functionalized particles may experience cross-linking, since the APTS molecule has three hydrolysable groups in its structure, which leads to the development of larger aggregates. Hydrodynamic diameter is also related to surface charge. According to the zeta potential *versus* pH curves in Figure 4, the value of zeta potential decreases in modulus from –25 mV (Fe_3O_4) to –7 mV (Fe_3O_4-APTS), and the absence of electrostatic repulsion may result in an aggregation process. The hydrodynamic diameter observed for free lipase was 7.6 nm, which is expected for small proteins. Due to crosslinking, which occurs when many supported enzymes combine throughout the reaction with glutaraldehyde, the immobilization step also displayed an increase in hydrodynamic diameter to 1088 nm. These results confirm the surface modification of the magnetic carrier with lipase.

TG was employed to determine the amount of enzymes that effectively bonded to the magnetic carrier. This determination was accomplished by comparing the mass loss between the samples of Fe_3O_4-APTS, Fe_3O_4-PPL, and free PPL (Figure 6). The mass losses below 200 °C can be attributed to the removal of water. For Fe_3O_4-APTS, mass loss was only 5.39% from 25 to 1000 °C, indicating good thermal resistance. The thermal behavior of Fe_3O_4-PPL exhibited a mass loss of 69.81% from 600 to 800 °C. For free PPL, 96.14% of organic composition was lost up to a temperature of 650 °C. This finding suggests that the immobilization may raise the temperature at which the enzyme decomposes to levels above those observed for free PPL. The remaining mass of the Fe_3O_4-PPL was 0.64 mg, representing 30.19% of the initial mass amount. By crossing the tangent lines, the TG curve can be verified; at a temperature of 794 ºC, they indicate a mass loss of 77.14%, therefore 22.86% is attributed to lipase on the magnetic support surface.

The hysteresis curves (Figure 7), recorded at 300 K, show remanent magnetization (Mr) and coercivity field (Hc) values of 1.31 emu g^{-1} and 49 Oe for Fe_3O_4-APTS, and 0.13 emu g^{-1} and 45 Oe for sample Fe_3O_4-PPL. In both samples, the small values of Mr and Hc indicate that a fraction of NPs is in the superparamagnetic regime and the rest is in the thermally blocked regime. The magnetization values measured at field strength of 1.5 T were 21.6 and 7.4 emu g^{-1} for Fe_3O_4-APTS and Fe_3O_4-PPL, respectively. To obtain the magnetization, the measured magnetic moment is normalized by the sample mass; thus, the magnetization of sample Fe_3O_4-PPL is smaller because of the mass of the PPL. Superparamagnetic NPs in the absence of a magnetic

Table 1. Average hydrodynamic diameter (D_h) and polydispersity index (PDI) for Fe_3O_4, Fe_3O_4-APTS, Fe_3O_4-PPL, and free PPL

Sample	D_h / nm	PDI
Fe_3O_4	234.1 ± 2.9	0.251
Fe_3O_4-APTS	554.1 ± 1.1	0.417
Fe_3O_4-PPL	1088 ± 45	0.490
Free PPL	7.6 ± 0.2	0.131

APTS: 3-aminopropyltriethoxysilane; PPL: porcine pancreatic lipase.

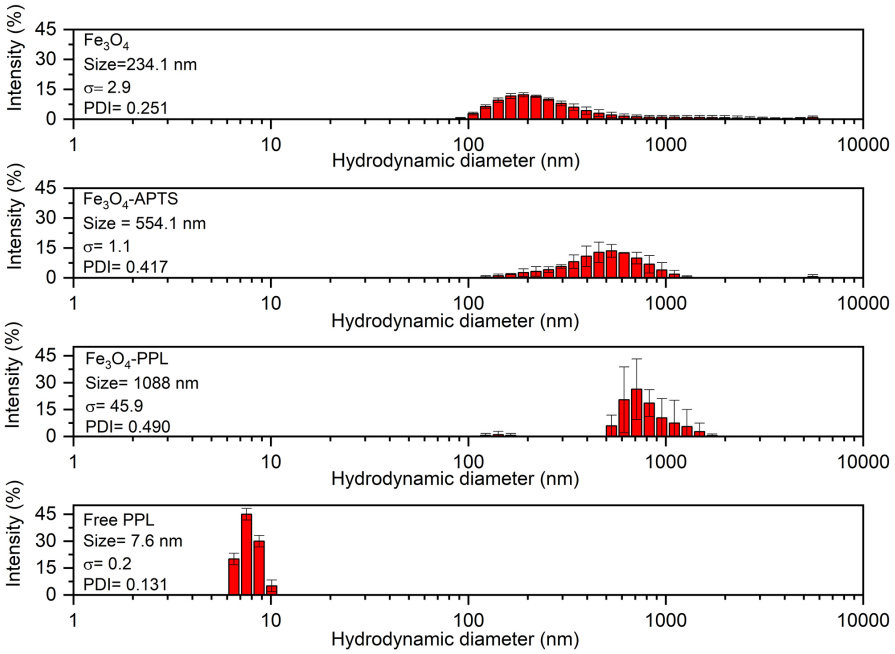

Figure 5. Hydrodynamic diameter distribution of Fe_3O_4, Fe_3O_4-APTS, Fe_3O_4-PPL, and free PPL.

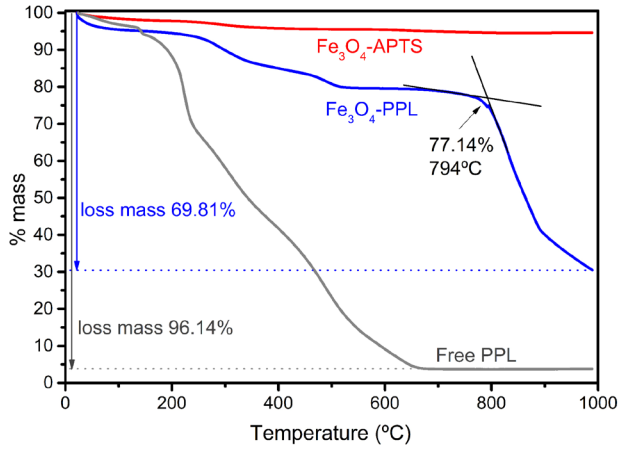

Figure 6. TG curves for Fe_3O_4-APTS, Fe_3O_4-PPL, and free PPL.

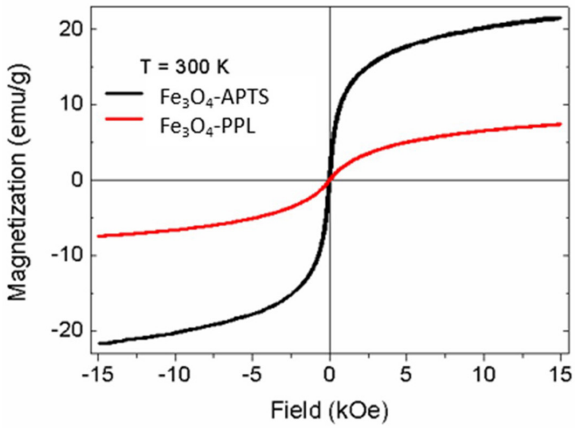

Figure 7. Hysteresis curves recorded at 300 K for samples Fe_3O_4-APTS and Fe_3O_4-PPL.

field behave like a non-magnetic system; however, in the presence of a field, they are strongly attracted by magnets. In this sense, the Fe_3O_4-PPL NPs may be removed from the aqueous dispersion by using a magnet.

Figure 8a shows the spectrum of sample Fe_3O_4-APTS, it was fit to two components: a doublet due to superparamagnetic NPs and a distribution of sextets ascribed to thermally blocked NPs (Table 2). The distribution of hyperfine magnetic field (H_{hf}) is displayed in Figure 8b and has its highest peak at 42 T; however, the magnetic field extends up to 50 T. The relative absorption area (RAA) of blocked particles was 65%. The distribution of H_{hf} shows fields noticeably smaller than expected for either bulk magnetite (46-49T) or maghemite (50 T).[36] This is because the whole system has not reached yet a blocked regime; in such a scenario, the H_{hf} would be larger, and it will be close to 49-50 T. The component doublet is related to superparamagnetic NPs, these are NPs with smaller size than the blocked ones. In both cases, the isomer shifts (IS) are in agreement with Fe^{3+}.[36]

Figure 8c shows the spectrum of sample Fe_3O_4-PPL. In order to fit the spectrum, we considered a sextet and a doublet. The sextet has H_{hf} and RAA of 48.8 T and 9%, respectively, meanwhile the doublet has RAA of 91%. This sample has a larger number of superparamagnetic NPs compared with sample Fe_3O_4-APTS.

Superparamagnetism is a property occurring in small, single-domain magnetic NPs without magnetic interaction, it is characterized by a blocking temperature (Tb), above which the NPs are superparamagnetic and below Tb the NPs are blocked. Factors like relaxation time of moments between the easy axis of magnetization (τ), magnetocrystalline anisotropy (K), and volume of NPs (V) affect the blocking temperature (T_b). In an ensemble of no interacting single-domain NPs, the magnetic moments in each NP experience a relaxation time (τ) is given by the Néel equation 3:

$$\tau = \tau_o e^{\frac{KV}{K_B T}} \quad (3)$$

where K_B is the Boltzmann constant, T is temperature, τ_o is a constant of the order of 10^{-9}-10^{-11} s. The relaxation is considered slow when τ is of the same order as the measuring time (τ_m), the value of τ_m depends on the experimental technique. For instance, τ_m is of 10 or 10^{-8} s for the techniques magnetometry or Mössbauer spectroscopy, respectively. In case of $\tau = \tau_m$, then $T = T_b$ (blocking temperature). In case of existing a magnetic interaction between NPs, the Néel equation is modified by adding a temperature term (T*) ascribed to interactions between NPs (see equation 4) as discussed by Allia *et al.*[42] in his model interacting superparamagnetic regime:

$$\tau_m = \tau_o e^{\frac{KV}{K_B\left(T+T^*\right)}} \quad (4)$$

The theory indicates that the actual magnetic moments on magnetic dipolar interacting NPs are systematically larger than those obtained considering the size of the NPs. The expectations of the model have been confirmed in granular Cu-Co alloys interacting superparamagnets[42] and Fe-oxide NPs,[43] among others.

Thus, the magnetic dipolar interparticle interaction becomes stronger when the NPs are too close, in this condition, a given NP feels the magnetic field from the neighbor NPs and their magnetic moments become blocked. This energy decreases when the NPs are moved far apart from each other. Therefore, the functionalization of magnetite NPs with PPL will increase the distance between two neighbor NPs by twice the size of the PPL molecule and, thus, more particles will turn superparamagnetic.

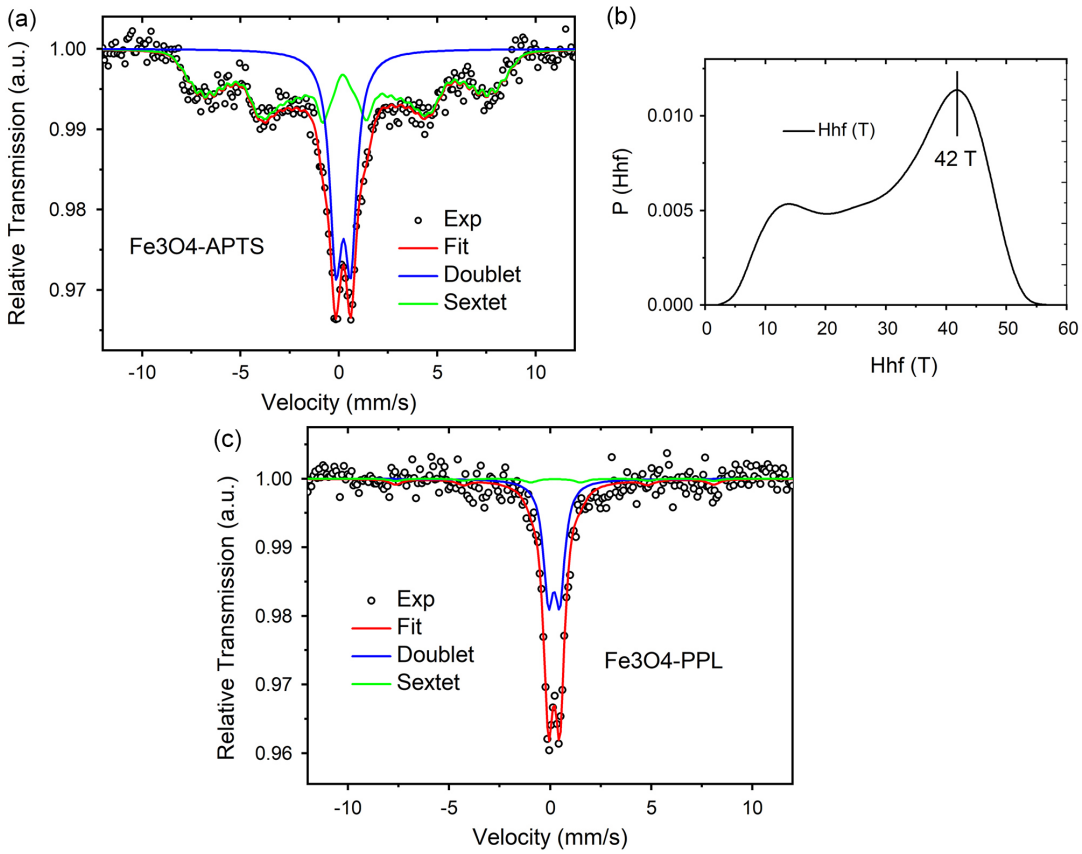

Figure 8. Mössbauer spectra recorded at 300 K for samples: (a) Fe_3O_4-APTS and (c) Fe_3O_4-PPL. (b) The histogram of the hyperfine magnetic field used to fit the spectrum of sample Fe_3O_4-APTS.

Table 2. Hyperfine parameters from fittings of spectra recorded at 300 K for samples Fe_3O_4-APTS and Fe_3O_4-PPL

	Fe_3O_4-APTS		Fe_3O_4-PPL	
	Doublet	Sextet	Doublet	Sextet
IS / (mm s^{-1})	0.343	0.321	0.301	0.350
QS / (mm s^{-1})	0.753	0.084	0.570	0.051
H_{hf} / T	–	44.2	–	48.8
RAA / %	35	65	91	5

IS: isomer shifts; QS: quadrupole splitting; H_{hf}: hyperfine magnetic field; RAA: relative absorption area; APTS: 3-aminopropyltriethoxysilane; PPL: porcine pancreatic lipase.

Catalytic activity of MCLEAs in olive oil transesterification

MNPs are excellent materials for use as carriers to immobilize enzymes since they can be stored for a long time and have high stability at neutral pH.[44] To determine the immobilization yield of enzymes on the surface of MNPs, the protein concentration dose was carried out. After 16 h of immobilization, Fe_3O_4-PPL has a protein concentration of 17.98 μg mL^{-1} compared to 22.78 μg mL^{-1} in free PPL, yielding an immobilization rate of 78.84%.

The effect of pH on the activity of the free and immobilized enzymes was evaluated. The highest activity of immobilized and free lipase was established as 100% and other pH conditions were listed as relative activities (Figure 9a). The results show that optimal activity for free PPL occurs at pH 7 while its Fe_3O_4-PPL form occurs at pH 8, indicating that immobilization influences the optimal pH. In addition, the immobilized derivative showed less variation in activity over a wide range of pH from 6 to 9, while the free enzyme showed a great loss of activity when reaching pH 8 and 9. Insoluble supports generally provide a unique microenvironment for immobilized enzymes, resulting in different performances in catalytic action. Some carrier properties, such as hydrophobicity, surface charge, and porosity, act to maintain the orientation and conformation of the enzymes on the carrier surface. Luo *et al.*[45] demonstrated through electrostatic analysis that most areas of the *Candida albicans* lipase, mainly the region around the active center, have a negative charge. Thus, the formation of covalent bonds between the enzyme and positively charged support might lead to conformational changes close to the active site and protect the active enzyme regions from pH changes.

The activities of free and immobilized lipase were also investigated concerning the temperature (Figure 9b). The Fe_3O_4-PPL sample did not show great activity variations

between 30 and 50 ºC. At 50 ºC, the immobilized derivative had an increase in its activity, reaching its maximum at an optimum temperature of 60 ºC. The results obtained from Fe_3O_4-PPL had better resistance to high temperatures than other supports used for PPL immobilization described in the literature, such as chitosan-SBA-15 nanocomposites and Fe_3O_4-chitosan.[46,47]

Thermal stabilities of the free and lipase immobilized were studied by measuring the activities of the lipase after incubation in phosphate buffer (Figure 9c). The results show that the soluble enzyme and the immobilized preparation retain almost 40% of the activity after 24 h of incubation at 60 ºC. Despite both curves had shown similar behavior, the immobilized sample shows advantages over the free one according to its reusability, as will be discussed in the next paragraphs. The storage temperature of 4 ºC was also evaluated during incubation of 24 h, and Fe_3O_4-PPL presented 62% of relative hydrolytic activity compared to free PPL with 59% (Figure 9d). According to the results, the Fe_3O_4-PPL loses activity more gradually after 12 h, whereas the activity decline in the free sample

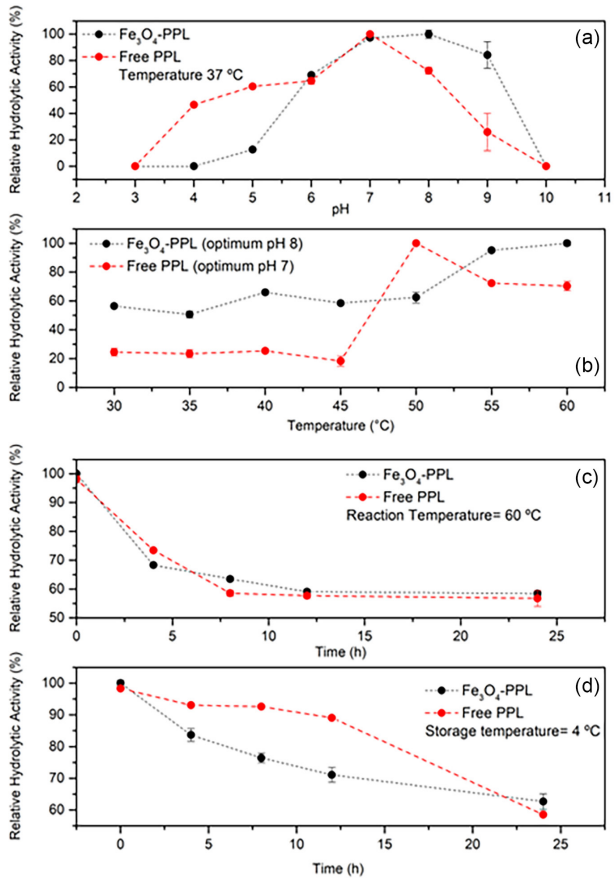

Figure 9. (a) Relative hydrolytic activity (%) of Fe_3O_4-PPL and free PPL as a function of pH. (b) Relative hydrolytic activity (%) of Fe_3O_4-PPL and free PPL as a function of temperature. (c) Thermal stability at 60 ºC for 24 h. (d) Storage stability at 4 ºC for 24 h.

is more pronounced. Despite the short storage stability in phosphate buffer, the immobilized sample shows better strength than free PPL.

The reusability of the biocatalyst has been also investigated to offset the cost of enzymes when compared to homogeneous and chemical catalysts. After each reaction, the immobilized lipase was recovered with a magnet and the next batch was carried out with a new substrate. Fe_3O_4-PPL showed a good ability to be used repeatedly (Figure 10). The initial activity before any recovery was set as 100% and, after 6 cycles, 61.37% of the initial activity of the derivative was maintained. Although the cycles lead to a reduction in activity, immobilization has the ability to lessen any modification to the enzyme's structure that could cause denaturation. This finding is good for reducing operational costs in real industrial processes. Similar outcome was attained in an earlier study using PPL immobilization on a magnetic graphene oxide platform, in which recyclability kept good activity (around 90%) for the first 6 cycles.[48] The literature reports similar behavior for immobilizations involving PPL and magnetic nanoparticles,[49] metal-organic frameworks (MOFs),[50] and zeolite supports,[51] where activity has kept above 50% after 6 cycles.

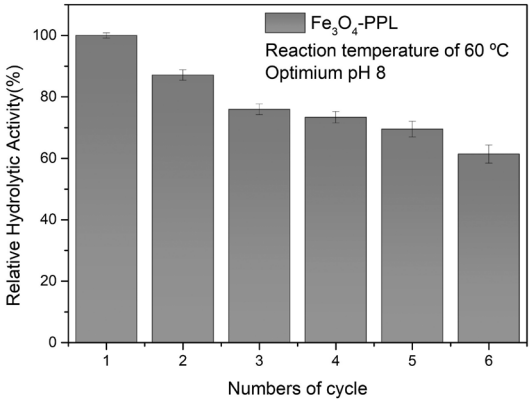

Figure 10. Relative hydrolytic activity (%) as a function of number of cycles using Fe_3O_4-PPL.

Conclusions

The obtaining and characterization of MCLEAs were successful. The functionalization and immobilization did not alter the crystal structure of the magnetic core. Besides, FTIR and zeta potential measurements confirmed functionalization with APTS and PPL immobilization. The enzyme immobilization also reveals a higher thermal resistance of MCLEA than compared with free lipase. The Mössbauer spectra of sample Fe_3O_4-PPL showed mainly a doublet, indicating that this sample is in the superparamagnetic regime. Regarding enzymatic activity, immobilized PPL presented higher activity at 60 °C than

free PPL. The free PPL had an optimum pH of 7.0, while the Fe_3O_4-PPL immobilized derivative gave an optimum pH of 8.0. The immobilized lipase exhibited remarkedly stability across a wide range of pH and temperature compared to the free one, along with good reusability after 6 cycles. The immobilization method has shown to be an excellent candidate for transesterification processes and the Fe_3O_4-PPL biocatalyst will be trialed in the production of biodiesel in future works.

Acknowledgments

This work was financially supported by Financier of Studies and Projects (FINEP); São Paulo State Research Support Foundation (FAPESP); National Council for Scientific and Technological Development (CNPQ); and Coordination for the Improvement of Higher Education Personnel (CAPES).

Author Contributions

Caroline O. da Rocha was responsible for conceptualization, data curation, formal analysis validation, visualization, writing original draft; Rodolfo D. Piazza for formal analysis, investigation, software, validation, visualization, writing original draft, review and editing; Caio C. dos Santos for formal analysis, investigation, software, validation, visualization, writing-review and editing; Guilherme N. Lucena for formal analysis, investigation, software, validation, visualization; Bruno E. Amantea for formal analysis, investigation, software, validation, visualization; Miguel Jafelicci Jr. for conceptualization, funding acquisition, project administration; Ariela V. de Paula for conceptualization, funding acquisition, project administration; Anselmo F. R. Rodriguez for formal analysis, investigation, writing-review and editing; Marco Antonio Morales for formal analysis, investigation, writing-review and editing; Rodrigo Fernando C. Marques for conceptualization, funding acquisition, project administration, writing-review and editing.

References

1. Mateo, C.; Palomo, J. M.; Fernandez-Lorente, G.; Guisan, J. M.; Fernandez-Lafuente, R.; *Enzyme Microb. Technol.* **2007**, *40*, 1451. [Crossref]
2. Mehrasbi, M. R.; Mohammadi, J.; Peyda, M.; Mohammadi, M.; *Renewable Energy* **2017**, *101*, 593. [Crossref]
3. Khoobbakht, G.; Kheiralipour, K.; Yuan, W.; Seifi, M. R.; Karimi, M.; *Renewable Energy* **2020**, *158*, 253. [Crossref]
4. Xie, W.; Huang, M.; *Renewable Energy* **2020**, *158*, 474. [Crossref]
5. Xie, W.; Wang, H.; *Renewable Energy* **2020**, *145*, 1709. [Crossref]
6. Badoei-dalfard, A.; Malekabadi, S.; Karami, Z.; Sargazi, G.; *Renewable Energy* **2019**, *141*, 874. [Crossref]
7. Villeneuve, P.; Muderhwa, J. M.; Graille, J.; Haas, M. J.; *J. Mol. Catal. B: Enzym.* **2000**, *9*, 113. [Crossref]
8. Pessela, B. C. C.; Dellamora-Ortiz, G.; Betancor, L.; Fuentes, M.; Guisán, J. M.; Fernandez-Lafuente, R.; *Enzyme Microb. Technol.* **2007**, *40*, 310. [Crossref]
9. Hanefeld, U.; Cao, L.; Magner, E.; *Chem. Soc. Rev.* **2013**, *42*, 6211. [Crossref]
10. Kim, J.; Grate, J. W.; Wang, P.; *Chem. Eng. Sci.* **2006**, *61*, 1017. [Crossref]
11. Fernández-Fernández, M.; Sanromán, M. Á.; Moldes, D.; *Biotechnol. Adv.* **2013**, *31*, 1808. [Crossref]
12. Mitchell, D. T.; Lee, S. B.; Trofin, L.; Li, N.; Nevanen, T. K.; Söderlund, H.; Martin, C. R.; *J. Am. Chem. Soc.* **2002**, *124*, 11864. [Crossref]
13. Andreescu, S.; Njagi, J.; Ispas, C.; *The New Frontiers of Organic and Composite Nanotechnology*, vol. 1, 1st ed.; Elsevier: London, UK, 2008, ch. 7.
14. Ma, Z.; Guan, Y.; Liu, H.; *J. Magn. Magn. Mater.* **2006**, *301*, 469. [Crossref]
15. Guo, Z.; Sun, Y.; *Biotechnol. Prog.* **2008**, *20*, 500. [Crossref]
16. Mohammadi, M.; Habibi, Z.; Dezvarei, S.; Yousefi, M.; Samadi, S.; Ashjari, M.; *Process Biochem.* **2014**, *49*, 1314. [Crossref]
17. Wu, P.; Zhu, J.; Xu, Z.; *Adv. Funct. Mater.* **2004**, *14*, 345. [Crossref]
18. Deng, Y.; Qi, D.; Deng, C.; Zhang, X.; Zhao, D.; *J. Am. Chem. Soc.* **2008**, *130*, 28. [Crossref]
19. Tran, D.-T.; Chen, C.-L.; Chang, J.-S.; *J. Biotechnol.* **2012**, *158*, 112. [Crossref]
20. Jaeger, K.-E.; Eggert, T.; *Curr. Opin. Biotechnol.* **2002**, *13*, 390. [Crossref]
21. Aravindan, R.; Anbumathi, P.; Viruthagiri, T.; *Indian J. Biotechnol.* **2007**, *6*, 141. [Crossref] accessed in December 2023
22. Hou, C. T.; *Handbook of Industrial Biocatalysis*, vol. 1, 1st ed.; CRC Press: Florida, USA, 2005, ch. 12.
23. Reis, P.; Holmberg, K.; Watzke, H.; Leser, M. E.; Miller, R.; *Adv. Colloid. Interface. Sci.* **2009**, *147-148*, 237. [Crossref]
24. Barbe, S.; Lafaquière, V.; Guieysse, D.; Monsan, P.; Remaud-Siméon, M.; André, I.; *Proteins: Struct., Funct., Bioinf.* **2009**, *77*, 509. [Crossref]
25. Kim, M. Il; Ham, H. O.; Oh, S.-D.; Park, H. G.; Chang, H. N.; Choi, S.-H.; *J. Mol. Catal. B: Enzym.* **2006**, *39*, 62. [Crossref]
26. Rai, M.; Ingle, A. P.; Pandit, R.; Paralikar, P.; Biswas, J. K.; da Silva, S. S.; *Catal. Rev.* **2019**, *61*, 1. [Crossref]
27. Bilal, M.; Iqbal, H. M. N.; Guo, S.; Hu, H.; Wang, W.; Zhang, X.; *Int. J. Biol. Macromol.* **2018**, *108*, 893. [Crossref]
28. Hou, C.; Zhu, H.; Li, Y.; Li, Y.; Ren, Y.; *J. Nanopart. Res.* **2014**, *16*, 2459. [Crossref]
29. Karimi, M.; *Biocatal. Agric. Biotechnol.* **2016**, *8*, 182. [Crossref]

30. Bassan, N.; Rodrigues, R. H.; Monti, R.; Tecelão, C.; Ferreira-Dias, S.; Paula, A. V.; *LWT* **2019**, *99*, 600. [Crossref]
31. Pinto, G. C.; Lucena, G. N.; Piazza, R. D.; Costa, J. M. L.; e Silva, E. T. C. C.; Gu, Y.; de Paula, A. V.; Silva, N. J. O.; Marques, R. F. C.; *Mater. Today Commun.* **2023**, *36*, 106441. [Crossref]
32. Rasband, W. S.; *ImageJ*, version 1.45s; U. S. National Institutes of Health, Bethesda, Maryland, USA, 2012.
33. Brand, R. A.; *Normos90*; Laboratórium für Argewandte Physik, Universität Duisburg, Duisburg, Germany, 1999.
34. Laurent, S.; Forge, D.; Port, M.; Roch, A.; Robic, C.; Vander Elst, L.; Muller, R. N.; *Chem. Rev.* **2008**, *108*, 2064. [Crossref]
35. Martins, M. A.; Trindade, T.; *Quim. Nova* **2012**, *35*, 1434. [Crossref]
36. Cornell, R. M.; Schwertmann, U.; *The Iron Oxides: Structure, Properties, Reactions, Occurences and Uses*, vol. 1, 2nd ed.; Wiley-VcH: Weinheim, Germany, 2003.
37. Kaya, H.; Ngo, D.; Gin, S.; Kim, S. H.; *J. Non-Cryst. Solids* **2020**, *527*, 119722. [Crossref]
38. Sizeland, K. H.; Hofman, K. A.; Hallett, I. C.; Martin, D. E.; Potgieter, J.; Kirby, N. M.; Hawley, A.; Mudie, S. T.; Ryan, T. M.; Haverkamp, R. G.; Cumming, M. H.; *Materialia* **2018**, *3*, 90. [Crossref]
39. Işık, C.; Saraç, N.; Teke, M.; Uğur, A.; *New J. Chem.* **2021**, *45*, 1984. [Crossref]
40. Paula, A. V.; Urioste, D.; Santos, J. C.; de Castro, H. F.; *J. Chem. Technol. Biotechnol.* **2007**, *82*, 281. [Crossref]
41. Bini, R. A.; Marques, R. F. C.; Santos, F. J.; Chaker, J. A.; Jafelicci Jr., M.; *J. Magn. Magn. Mater.* **2012**, *324*, 534. [Crossref]
42. Allia, P.; Coisson, M.; Tiberto, P.; Vinai, F.; Knobel, M.; Novak, M. A.; Nunes, W. C.; *Phys. Rev. B* **2001**, *64*, 144420. [Crossref]
43. Allia, P.; *J. Phys.: Conf. Ser.* **2014**, *521*, 012008. [Crossref]
44. Lucena, G. N.; dos Santos, C. C.; Pinto, G. C.; Piazza, R. D.; Guedes, W. N.; Jafelicci Jr., M.; de Paula, A. V.; Marques, R. F. C.; *J. Magn. Magn. Mater.* **2020**, *516*, 167326. [Crossref]
45. Luo, M.; Wang, L.; Chen, G.; Zhao, J.; *Colloids Surf., B* **2023**, *225*, 113286. [Crossref]
46. Xiang, X.; Ding, S.; Suo, H.; Xu, C.; Gao, Z.; Hu, Y.; *Carbohydr. Polym.* **2018**, *182*, 245. [Crossref]
47. Suo, H.; Xu, L.; Xu, C.; Chen, H.; Yu, D.; Gao, Z.; Huang, H.; Hu, Y.; *Int. J. Biol. Macromol.* **2018**, *119*, 624. [Crossref]
48. Pinto, G. C.; Brandt, J. V.; Piazza, R. D.; dos Santos, C. C.; Lucena, G. N.; de Paula, A. V.; Jafelicci Jr., M.; Marques, R. F. C.; *ECS J. Solid State Sci. Technol.* **2021**, *10*, 65008. [Crossref]
49. Zhu, Y.-T.; Ren, X.-Y.; Liu, Y.-M.; Wei, Y.; Qing, L.-S.; Liao, X.; *Mater. Sci. Eng.: C* **2014**, *38*, 278. [Crossref]
50. Chen, X.; Xue, S.; Lin, Y.; Luo, J.; Kong, L.; *Anal. Chim. Acta* **2020**, *1099*, 94. [Crossref]
51. Taghizadeh, T.; Ameri, A.; Talebian-Kiakalaieh, A.; Mojtabavi, S.; Ameri, A.; Forootanfar, H.; Tarighi, S.; Faramarzi, M. A.; *Int. J. Biol. Macromol.* **2021**, *166*, 1301. [Crossref]

Submitted: August 23, 2023
Published online: January 10, 2024